Letter   Editors' Suggestion   Featured in Physics

Sea urchin sperm exploit extremum seeking control to find the egg

Mahmoud Abdelgalil [*]

Department of Mechanical and Aerospace Engineering, University of California, Irvine, California 92697, USA

Yasser Aboelkassem [†]

College of Innovation and Technology, University of Michigan at Flint, Flint, Michigan 48502, USA
and Michigan Institute for Data Science, University of Michigan, Ann Arbor, Michigan 48109, USA

Haithem Taha[‡]

Department of Mechanical and Aerospace Engineering, University of California, Irvine, California 92697, USA

Sperm cells perform extremely demanding tasks with minimal capabilities. The cells must quickly navigate in a noisy environment to find an egg within a short time window for successful fertilization without any global positioning information. Many research efforts have been dedicated to derive mathematical principles that explain their superb navigation strategy. Here we show that the navigation strategy of sea urchin sperm, also known as helical klinotaxis, is a natural implementation of a well-established adaptive control paradigm known as extremum seeking. This bridge between control theory and the biology of taxis in microorganisms is expected to deepen our understanding of the process. For example, the formulation leads to a coarse-grained model of the signaling pathway that offers new insights on the peculiar switching-like behavior between high- and low-gain steering modes observed in sea urchin sperm. Moreover, it may guide engineers in developing bioinspired miniaturized robots with minimal sensors.

I. INTRODUCTION

Source seeking, a well-studied topic in the control community [1], is the problem of locating an object that emits a scalar measurable signal (e.g., chemical concentration, sound, heat, etc.), typically without global positioning information. Many organisms are routinely faced with the source seeking problem. A well-studied example is that of sperm chemotaxis [2,3]. To locate an egg in open water, sea urchin sperm evolved to swim up the gradient of the concentration field established by the diffusion of a species-specific chemoattractant, a sperm-activating peptide (SAP), secreted by the eggs [3]. Unlike the inherently stochastic bacterial chemotaxis, the navigation strategy of sea urchin sperm can be reasonably described in a deterministic fashion: The cells employ the mean curvature of the flagellum, regulated by intracellular Ca^{2+}, as a steering mechanism to swim in circular paths that drift in the direction of the gradient in two dimensions (2D), and in helical paths that align with the gradient in three dimensions (3D) [2,4–6]. This feedback mechanism is mediated by a complex signaling pathway that regulates the influx and efflux of Ca^{2+} in the cell [7,8].

In this letter, we revisit sperm chemotaxis from the perspective of control theory. We frame the search for the egg as a source seeking problem, then we show that the 3D navigation strategy of sea urchin sperm, also known as helical klinotaxis,

is in fact a natural implementation of a well-established adaptive control paradigm known as extremum seeking [1,9,10]. We illustrate this connection by establishing a one-to-one correspondence between the key components of the navigation strategy of sea urchin sperm cells and the hallmark features of an extremum seeking solution to the source seeking problem. Based on this formulation, we propose a coarse-grained minimal dynamical description that captures the crucial features of the chemotactic signaling pathway, including the peculiar behavior of sea urchin sperm cells where they seem to switch between two distinct navigation modes: (i) the "on response," which is a low-gain steering mode when the average velocity vector of the cell is mostly aligned with the gradient, and (ii) the "off response," which is a high-gain steering mode otherwise [6]. Previous models employed a threshold-based switching logic to account for this behavior [6]. The threshold defining the discontinuous switching boundary was later determined as the solution to an optimal decision problem [11]. Here, we show that the behavior can arise from a continuous dynamical description in a simpler way: it arises as a consequence of the motion pattern and a time-scale separation between the proposed dynamics of the signaling pathway and the average motion. In particular, the proposed model does not exploit any information other than the perceived instantaneous local concentration.

II. A PRIMER ON EXTREMUM SEEKING

We begin with a brief exposition of extremum seeking (ES) control. ES is an adaptive control technique designed to steer a

[*]maabdelg@uci.edu
[†]yassera@umich.edu
[‡]hetaha@uci.edu
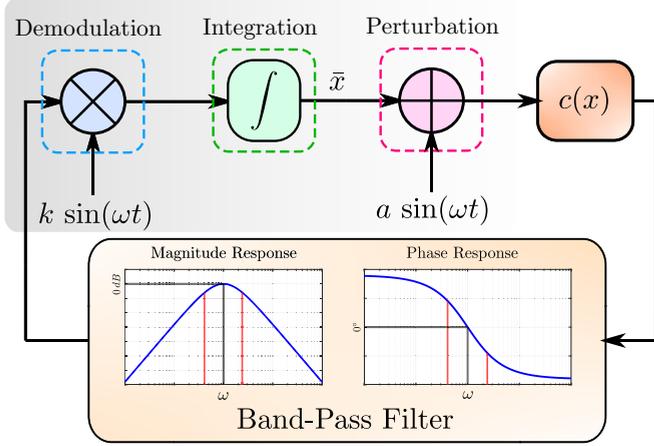
FIG. 1. A block diagram description of the simplest extremum seeking control scheme as represented by Eqs. (1).

dynamical system towards the extremum of an objective function that depends on the state of the system, without access to information about the gradient of the function (only the value of the objective function is available for measurement at each instant in time). The first ES control law can be traced back to the century-old paper due to Leblanc [12], but the recent interest in ES control was sparked by Krstić's seminal paper [13]. In the simplest setting, an ES controller is designed to find the optimal value of a single-variable static objective function by dynamically estimating the gradient. Let $c(x)$ be the objective function, and consider the following dynamical system [14]:

$$x = \bar{x} + a \sin(\omega t), \quad \dot{\bar{x}} = 2 \zeta k \sin(\omega t), \tag{1a}$$

$$\dot{\zeta}_1 = \omega (\zeta_2 - \zeta_1), \quad \dot{\zeta}_2 = \omega (c(x) - \zeta_2), \quad \zeta = \zeta_2 - \zeta_1, \tag{1b}$$

which is depicted in the block diagram [15] presented in Fig. 1, where $\bar{x}$ is the estimate of the optimal value of the independent variable x, ζ_1 and ζ_2 are the states of a bandpass filter centered around the constant frequency ω, and k, a are tuning parameters. The flow of the block diagram in Fig. 1 can be traced as follows. First, a sinusoidal perturbation is injected to sample the objective function near the estimate $\bar{x}$. Using Taylor expansion, the instantaneous cost can be written as

$$c(x) = c(\bar{x}) + \frac{dc(\bar{x})}{d\bar{x}} a \sin(\omega t) + O(a^2). \tag{2}$$

We observe how the gradient appears as the amplitude of the sinusoidal perturbation. In engineering terms, injecting the perturbation around the current estimate $\bar{x}$ modulates the local gradient information on the amplitude of the sinusoidal carrier signal $\sin(\omega t)$. Therefore, to extract the gradient information, the measured objective function $c(x)$ goes through a bandpass filter centered around the frequency ω as defined by Eq. (1b). The output of the filter ζ can be approximated in the quasisteady sense by

$$2\zeta \approx 2\zeta_{QS} = \frac{dc(\bar{x})}{d\bar{x}} a \sin(\omega t), \tag{3}$$

Next, the gradient information is demodulated (i.e., extracted from the carrier signal) through multiplication with another

sinusoid having the same frequency and phase as the carrier signal:

$$2 \zeta k \sin(\omega t) = \frac{a k}{2} \frac{dc(\bar{x})}{d\bar{x}} [1 - \cos(2\omega t)], \tag{4}$$

where the time average of the right-hand side of Eq. (4) is proportional to the gradient. Finally, the demodulated gradient information is used in adjusting the current estimate $\bar{x}$. Through a simple averaging argument, we obtain that the estimate $\bar{x}$ evolves on average according to

$$\dot{\bar{x}} \approx \overline{2 \zeta_{QS} k \sin(\omega t)} = \frac{a k}{2} \frac{dc(\bar{x})}{d\bar{x}}, \tag{5}$$

where the overline $\overline{}$ indicates the time average of the overlined quantity. That is, the estimate $\bar{x}$ evolves, in a quasisteady average sense, along the gradient of the objective function under the extremum seeking control law [Eq. (1)]. The interested reader is referred to Refs. [13,14,16] for more details.

III. MODELING THE SPERM MOTION

We now turn our attention to the motion of the sperm cell. Swimming in a low Reynolds number is dominated by viscous forces, which enables the use of kinematic models as a good approximation to the motion of microswimmers, including sperm cells [17]. The kinematics of a rigid body are given by

$$\dot{\mathbf{x}} = \mathbf{R}\mathbf{v}, \quad \dot{\mathbf{R}} = \mathbf{R}\hat{\boldsymbol{\omega}}, \tag{6}$$

where the vectors $\mathbf{v}$ and $\boldsymbol{\omega}$ are the linear and angular velocity vectors in the body frame, $\hat{\boldsymbol{\omega}}$ denotes the skew-symmetric matrix corresponding to the angular velocity vector $\boldsymbol{\omega}$, $\mathbf{x}$ is the instantaneous position of the body with respect to the origin of a fixed frame of reference, and $\mathbf{R}$ is the instantaneous rotation matrix that relates the body frame to the fixed frame. In sea urchin sperm, the mean curvature of the flagellar beating pattern, which is regulated by the chemotactic signaling pathway, controls the angular velocities in the body frame [3,4]. A common model of the effect of the chemotactic signaling pathway on the swimming kinematics of sea urchin sperm is given by the relations

$$\mathbf{v} = [v \quad 0 \quad 0]^{\mathsf{T}}, \quad \boldsymbol{\omega} = [\omega_{\parallel} \quad 0 \quad \omega_{\perp}]^{\mathsf{T}}, \tag{7}$$

where $v > 0$ is constant and the angular velocity components $\omega_{\parallel}$ and $\omega_{\perp}$ are given by

$$\omega_{\parallel} = \omega_{\parallel 0} + \omega_{\parallel 1}\eta, \quad \omega_{\perp} = \omega_{\perp 0} + \omega_{\perp 1}\eta, \tag{8}$$

with $\omega_{\perp 0}, \omega_{\perp 1}, \omega_{\parallel 0}, \omega_{\parallel 1}$ as constant coefficients, and η is a dynamic feedback term representing the effect of the signaling pathway [2,6,18].

IV. AN EXTREMUM SEEKING LOOP

The constant forward velocity $v > 0$, along with the constant angular velocity components $\omega_{\parallel 0}$ and $\omega_{\perp 0}$, lead to a periodic swimming pattern, a helical trajectory. The sign of $\omega_{\parallel 0}$ and $\omega_{\perp 0}$ determine the handedness of the helical trajectory. For simplicity, we consider the case in which both $\omega_{\parallel 0}$ and $\omega_{\perp 0}$ are positive. The geometry of helical swimming [see Fig. 2(a)] suggests decomposing the motion into an average
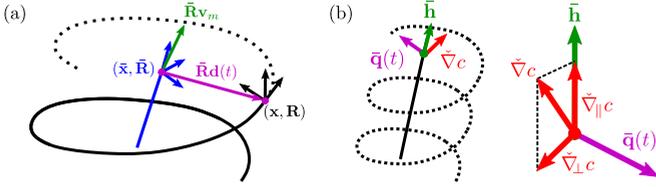
FIG. 2. The geometry of helical swimming. (a) The helical nature of the trajectory suggests decomposing the motion $(\mathbf{x}, \mathbf{R})$ into an average part along the helical centerline $(\bar{\mathbf{x}}, \bar{\mathbf{R}})$ and a periodic excursion $\bar{\mathbf{R}}\mathbf{d}(t)$ that is orthogonal to the centerline. (b) The direction of the gradient $\check{\nabla}c$ can be decomposed into two parts, one along the helical centerline $\bar{\mathbf{h}}$ (denoted as $\check{\nabla}_{\parallel}c$), and another orthogonal to it (denoted as $\check{\nabla}_{\perp}c$) which is contained in the same plane as the direction $\bar{\mathbf{q}}(t)$ of the periodic excursion $\bar{\mathbf{R}}\mathbf{d}(t)$.

part and an oscillatory part. We define the average instantaneous position $\bar{\mathbf{x}}$ and orientation $\bar{\mathbf{R}}$ of the cell as

$$\mathbf{R}_0(t) = \exp(\widehat{\boldsymbol{\omega}}_0 t), \quad \bar{\mathbf{R}} = \mathbf{R}\mathbf{R}_0(t)^{\mathsf{T}}, \quad (9a)$$

$$\bar{\mathbf{x}} = \mathbf{x} - \bar{\mathbf{R}}\mathbf{d}(t), \quad (9b)$$

where the vector $\boldsymbol{\omega}_0$ is given by

$$\boldsymbol{\omega}_0 = [\omega_{\parallel 0} \quad 0 \quad \omega_{\perp 0}]^{\mathsf{T}} \quad (10)$$

and the vector $\mathbf{d}(t)$ is the perturbation in the position due to the helical swimming pattern, and is defined by

$$\mathbf{v}_m = \overline{\mathbf{R}_0(t)\mathbf{v}}, \quad \mathbf{d}(t) = \int (\mathbf{R}_0(t)\mathbf{v} - \mathbf{v}_m)dt. \quad (11)$$

In particular, the periodic perturbation vector $\mathbf{d}(t)$ and the average velocity vector $\mathbf{v}_m$ are orthogonal. The evolution of the average motion variables $\bar{\mathbf{x}}$ and $\bar{\mathbf{R}}$ is governed by the following system of differential equations with periodic coefficients:

$$\dot{\bar{\mathbf{x}}} = \bar{\mathbf{R}}\mathbf{v}_\eta(t)\eta + \bar{\mathbf{R}}\mathbf{v}_m, \quad \mathbf{v}_\eta(t) = \mathbf{d}(t) \times \boldsymbol{\omega}_\eta(t), \quad (12a)$$

$$\dot{\bar{\mathbf{R}}} = \bar{\mathbf{R}}\widehat{\boldsymbol{\omega}}_\eta(t)\eta, \quad \boldsymbol{\omega}_\eta(t) = \mathbf{R}_0(t)\boldsymbol{\omega}_1, \quad (12b)$$

where the vector $\boldsymbol{\omega}_1$ is given by

$$\boldsymbol{\omega}_1 = [\omega_{\parallel 1} \quad 0 \quad \omega_{\perp 1}]^{\mathsf{T}}. \quad (13)$$

Under the assumption that $|\mathbf{d}(t)| \ll 1$, the instantaneous local concentration $c(\mathbf{x})$ can be approximated as a Taylor series in terms of the average motion variables $\bar{\mathbf{x}}$ and $\bar{\mathbf{R}}$ using Eq. (9b):

$$c(\mathbf{x}) \approx c(\bar{\mathbf{x}}) + \nabla c(\bar{\mathbf{x}})^{\mathsf{T}}\bar{\mathbf{R}}\mathbf{d}(t). \quad (14)$$

Clearly, the helical swimming pattern modulates the local gradient information on the amplitude of the perturbation $\bar{\mathbf{R}}\mathbf{d}(t)$, similar to the perturbation stage of the ES control loop. The amplitude of the periodic component $\nabla c(\bar{\mathbf{x}})^{\mathsf{T}}\bar{\mathbf{R}}\mathbf{d}(t)$ of the instantaneous local concentration [Eq. (14)] is proportional to the component of the local gradient that is orthogonal to the average swimming direction as defined by $\bar{\mathbf{R}}\mathbf{v}_m$.

It is well known that microorganisms that swim in helical trajectories, including sea urchin sperm, can align the axis of their helical trajectory with the gradient by periodically varying the angular velocities of the cell with the same frequency of the helical trajectory [4,18]. That is, a sperm cell can align its swimming direction with the gradient provided that the signaling pathway is able to extract the periodic component
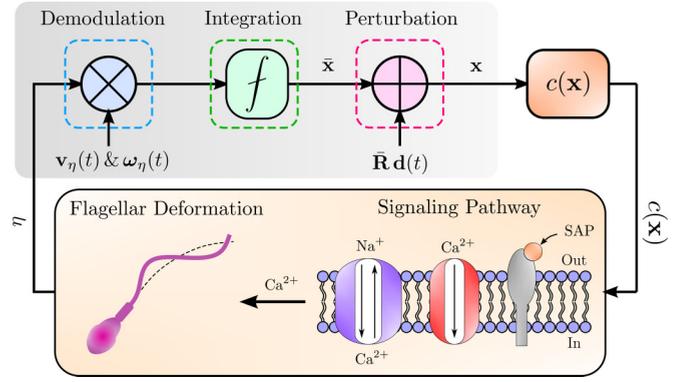
FIG. 3. A block diagram description of the chemotactic navigation of sperm represented by Eqs. (9) and (12).

of the instantaneous local concentration, similar to the role of the filter in the ES control loop. This implication about the role of the signaling pathway is one of the main outcomes of the connection between chemotaxis and ES, as proposed in this paper.

Going back to the governing equations of the kinematics [Eqs. (12)], we see that the feedback signal η multiplies the periodic feedback coefficients $\mathbf{v}_\eta(t)$ and $\boldsymbol{\omega}_\eta(t)$. Consequently, the local gradient information carried on the periodic component in the signal η is demodulated into the nonzero average component of the product signals $\boldsymbol{\omega}_\eta(t)\eta$ and $\mathbf{v}_\eta(t)\eta$, similar to the demodulation stage of the ES control loop.

Finally, the demodulated local gradient information passes through the kinematics of the motion represented by Eqs. (12), which is responsible for biasing the motion in the direction of the gradient. The closed-loop behavior of the nonholonomic integrator defined by the kinematics is investigated in the next section. A block diagram description of the dynamical Eqs. (12) representing the navigation strategy of sea urchin sperm is shown in Fig. 3, where the special integration symbol $\int$ denotes the nonholonomic kinematic integrator corresponding to Eqs. (12). The isomorphism between the block diagrams in Figs. 1 and 3 clearly reveals the connection between sperm chemotaxis and extremum seeking. We remark that the signaling pathway is more complicated than the simple input-output depiction shown in Fig. 3 (see Ref. [3] for more details).

It is noteworthy that the 2D version of the model [Eqs. (6)–(8) (i.e., when $\omega_{\parallel} = 0$ and the motion is restricted to a plane) is a well-studied kinematic model in the control community known as the unicycle model. Remarkably, the trajectories generated by an ES-based algorithm for the unicycle model, which was recently proposed in Refs. [9,10] independently from the literature on sperm chemotaxis, are astonishingly similar to the actual trajectories of sea urchin sperm in shallow observation chambers [19].

V. CHEMOTACTIC RESPONSE AND CLOSED-LOOP BEHAVIOR

The evident one-to-one correspondence between the key components of the navigation strategy of sea urchin sperm and ES control immediately clarifies the role of the signaling

v	$\omega_{\parallel 0}$	$\omega_{\parallel 1}$	$\omega_{\perp 0}$	$\omega_{\perp 1}$	μ	σ	$\eta(t_0)$	$\zeta(t_0)$	$\rho(t_0)$
3.07	3.07	2.30	8.91	1.00	3.07	9.42	0.00	$c(\mathbf{x}_0)$	5.00
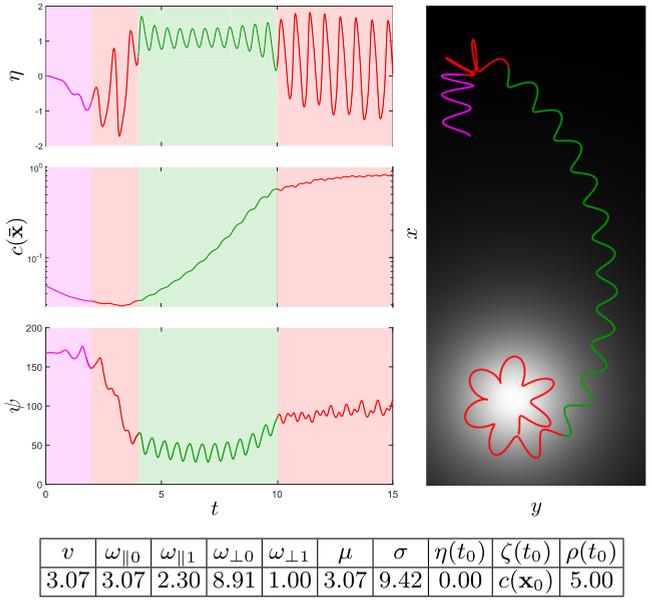
FIG. 4. The three cases of the behavior of the signaling pathway illustrated on a sample trajectory projected on the xy-plane, the response η, the average instantaneous concentration $c(\bar{\mathbf{x}})$, and the angle $\psi = \cos^{-1}(\bar{\mathbf{h}}^{\mathsf{T}} \check{\nabla} c)$ (in degrees) between the gradient and the average direction of motion $\bar{\mathbf{h}}$, in a radial concentration field $c(\mathbf{x}) = 1/(1 + 0.5|\mathbf{x}|^2)$. The initial position is taken as $\mathbf{x}_0 = (6, 1, 0)$, and the initial orientation is $\mathbf{R}(t_0) = \exp(2\pi \hat{\mathbf{e}}_2/5)$, where $\hat{\mathbf{e}}_2 = (0, 1, 0)$. The rest of the initial conditions and parameter values are in the table.

pathway: it must act as an adaptive bandpass filter attuned to the frequency of the swimming pattern of the cell. Motivated by this observation, and building upon previous phenomenological models [2,6], we propose the following coarse-grained dynamical description of the signaling pathway:

$$\sigma \dot{\xi} = s(t) - \xi, \tag{15a}$$

$$\mu \dot{\eta} = \rho \dot{\xi} - \eta^3, \tag{15b}$$

$$\mu \dot{\rho} = \rho - \rho \eta^2, \tag{15c}$$

where μ and σ are positive constants such that $\sigma < \mu$, and $s(t)$ is the input to the model, which represents the time-varying external stimulus to which the pathway is exposed due to the binding of SAP molecules with the receptors. Without accounting for noise, the stimulus $s(t)$ is customarily approximated by

$$s(t) \approx \lambda c(\mathbf{x}) \tag{16}$$

for some positive proportionality constant λ [2,6]. The proposed model possesses three essential dynamical features: excitation, relaxation, and adaptation. The excitation is modelled by Eq. (15a), which acts as a differentiator that detects changes in the local concentration. The relaxation is modeled by Eq. (15b), which brings the response η back to resting levels when there is no change in the stimulus. Finally, the adaptation is modeled by Eq. (15c), which adjusts the sensitivity of the pathway to the stimulus. A sample trajectory of Eqs. (6)–(8) and (15) is shown in Fig. 4 along with the time history of the average local concentration $c(\bar{\mathbf{x}})$, the steering

response η, and the angle ψ between the gradient and the average swimming direction.

We now analyze the closed-loop behavior when the dynamics of the pathway is given by the proposed dynamical system [Eq. (15)] using analytical calculations based on linear response theory and averaging, similar to Refs. [2,6]. The details of calculations in this section can be found in the Supplemental Material [20]. In the parametric regime where $\sigma|\mathbf{v}_m| \ll \mu|\mathbf{v}_m| \ll \sigma|\boldsymbol{\omega}_0| \approx O(1)$, there is a large time-scale separation between the dynamics of average motion [Eq. (12)] in the absence of feedback and the dynamics of the pathway [Eq. (15)]. Consequently, we may approximate the response η due to the time-varying local concentration [Eq. (14)] by the quasisteady response,

$$\eta_{\mathrm{QS}} = \frac{\bar{\mathbf{h}}^{\mathsf{T}} \check{\nabla} c + \sqrt{2}\,\beta\,\bar{\mathbf{q}}(t + t_\phi)^{\mathsf{T}} \check{\nabla}_\perp c}{\sqrt{|\check{\nabla}_\parallel c|^2 + \beta^2 |\check{\nabla}_\perp c|^2}}, \tag{17}$$

where $\beta = \gamma(\omega)|\mathbf{d}(t)|/(\mu\sqrt{2}|\mathbf{v}_m|)$; $t_\phi = \phi(\omega)/\omega$, with $\gamma(\omega)$ and $\phi(\omega)$ being the gain and phase contributions of the linear part of the system [Eq. (15)] at the frequency $\omega = |\boldsymbol{\omega}_0|$ (exact expressions can be found in the Supplemental Material [20]); and $\check{\nabla} c = \nabla c(\bar{\mathbf{x}})/|\nabla c(\bar{\mathbf{x}})|$ is a unit vector in the direction of the gradient, and we used the following shorthand notations:

$$\bar{\mathbf{h}} = \bar{\mathbf{R}}\mathbf{v}_m/|\mathbf{v}_m|, \quad \bar{\mathbf{q}}(t) = \bar{\mathbf{R}}\mathbf{d}(t)/|\mathbf{d}(t)|,$$

$$\check{\nabla}_\parallel c = \bar{\mathbf{h}}\,\bar{\mathbf{h}}^{\mathsf{T}} \check{\nabla} c, \quad \check{\nabla}_\perp c = \check{\nabla} c - \check{\nabla}_\parallel c$$

to simplify the expression [see Fig. 2(b) for a geometric illustration of the introduced variables]. Notably, the quasisteady response [Eq. (17)] is independent of the ambient concentration $c(\mathbf{x}_0)$ and the stimulus proportionality constant λ, which are irrelevant information from a chemotactic perspective. If we close the loop by replacing η with the quasisteady approximation η_{QS}, an intricate averaging analysis on the fast time scale $\tau = \omega t$ when $\omega \gg 1$ for the system of Eqs. (12a) and (12b) coupled with Eq. (17) leads to the following averaged quasisteady equations:

$$\dot{\bar{\mathbf{x}}}^{\mathsf{T}} \bar{\mathbf{h}} = \frac{v\,\omega_{\parallel 0}}{\omega}\left(1 + \frac{\omega_{\perp 0}^2 \omega_{\parallel 1}}{\omega^2 \omega_{\parallel 0} \alpha}\bar{\mathbf{h}}^{\mathsf{T}} \check{\nabla} c\right), \tag{18a}$$

$$\dot{\bar{\mathbf{h}}}^{\mathsf{T}} \check{\nabla} c = \frac{\gamma(\omega)\,\omega_{\perp 0}^2 \omega_{\parallel 1}}{2\mu\omega^2 \omega_{\parallel 0}\alpha} \cos[\phi(\omega)]|\check{\nabla}_\perp c|^2, \tag{18b}$$

$$\alpha = \sqrt{|\check{\nabla}_\parallel c|^2 + \beta^2 |\check{\nabla}_\perp c|^2}. \tag{18c}$$

Equation (18a) expresses the speed along the average direction of motion $\bar{\mathbf{h}}$, while Eq. (18b) presents the rate of alignment of the average direction of motion $\bar{\mathbf{h}}$ with the gradient. We now analyze the qualitative dynamic behavior of the quasisteady averaged Eqs. (18) by considering three events and the corresponding response. The first event (the segments highlighted in green in Fig. 4) is when the average swimming direction $\bar{\mathbf{h}}$ is mostly aligned with the gradient (i.e., $\beta|\check{\nabla}_\perp c| \ll \bar{\mathbf{h}}^{\mathsf{T}}\check{\nabla}_\parallel c \approx 1$), in which case the response η_{QS} is approximately given by

$$\eta_{\mathrm{QS}} \approx 1 + \sqrt{2}\,\beta\,\bar{\mathbf{q}}(t + t_\phi)^{\mathsf{T}}\check{\nabla}_\perp c, \tag{19}$$

where the second term is small compared to 1 (i.e., the periodic component is attenuated relative to the slope of the ramp

component), and the change in the misalignment between the average swimming direction and the gradient is minor. Moreover, the net motion along the average swimming direction $\bar{\mathbf{h}}$ is sped up:

$$\dot{\mathbf{x}}^\intercal \bar{\mathbf{h}} \approx \frac{v\,\omega_{\|0}}{\omega}\left(1 + \frac{\omega_{\|1}\omega_{\perp 0}^2}{\omega_{\|0}\omega^2}\right). \tag{20}$$

The second event (the segments highlighted in purple in Fig. 4) is when the average swimming direction is almost opposite of the gradient (i.e., $\bar{\mathbf{h}}^\intercal \check{\nabla}_\| c \approx -1$), in which case the response is approximately given by

$$\eta_{\mathrm{QS}} \approx -1 + \sqrt{2}\,\beta\,\bar{\mathbf{q}}(t+t_\phi)^\intercal \check{\nabla}_\perp c, \tag{21}$$

where once again the periodic term is small. However, the net speed along the average swimming direction $\bar{\mathbf{h}}$ is reduced:

$$\dot{\mathbf{x}}^\intercal \bar{\mathbf{h}} \approx \frac{v\,\omega_{\|0}}{\omega}\left(1 - \frac{\omega_{\|1}\omega_{\perp 0}^2}{\omega_{\|0}\omega^2}\right). \tag{22}$$

That is, when the motion is opposite of the gradient, the net motion along the average swimming direction $\bar{\mathbf{h}}$ is slowed down, thereby reducing the helical pitch of the trajectory. This helical pitch reduction can be observed in the purple segment of the trajectory in Fig. 4. Moreover, the average swimming direction defined by $\bar{\mathbf{h}}^\intercal \check{\nabla}_\| c = -1$ is unstable, so any slight misalignment triggers the transition towards the stable average swimming direction defined by $\bar{\mathbf{h}}^\intercal \check{\nabla}_\| c \approx 1$.

The third event (the segments highlighted in red in Fig. 4) is when the average swimming direction $\bar{\mathbf{h}}$ is orthogonal to the gradient (i.e., $\bar{\mathbf{h}}^\intercal \check{\nabla}_\| c \approx 0$ and $|\check{\nabla}_\| c| \approx 1$), in which case the quasisteady response η_{QS} is dominated by the periodic component in the local concentration,

$$\eta_{\mathrm{QS}} \approx \sqrt{2}\,\bar{\mathbf{q}}(t+t_\phi)^\intercal \check{\nabla}_\perp c, \tag{23}$$

and the alignment between the average swimming direction and the gradient is increased at a peak rate,

$$\dot{\bar{\mathbf{h}}}^\intercal \check{\nabla} c \approx \frac{\omega_{\perp 0}\omega_{\|1}}{\sqrt{2}\,\omega}\cos[\phi(\omega)]. \tag{24}$$

We remark that near the maximum concentration, the gradient vanishes, and the behavior of the system is dominated by second-order effects, due to the Hessian of the concentration field, which are neglected here.

VI. DISCUSSION

Helical klinotaxis is a ubiquitous mode of taxis in microorganisms. In this study, we used sperm chemotaxis in sea urchins to highlight extremum seeking control as an underlying principle behind helical klinotaxis. This connection sheds light on the role played by the chemotactic signaling pathway and emphasizes the characterization of its dynamics as an adaptive bandpass filter. Moreover, we showed that the switching-like behavior of sea urchin sperm can arise from a continuous dynamical description [Eq. (15)] without an explicit discontinuous switching logic as in previously proposed models [6,11]. The key feature of the model [Eq. (15)] is that the gain ρ adapts to the filtered stimulus $\dot{\xi}$ rather than the stimulus $s(t)$ directly. As a consequence, the ambient concentration levels do not alter the behavior of the model significantly. The forward velocity v of the cell is treated as a constant in the kinematic model [Eqs. (6)–(8)]. Yet, the cell is able to adjust the speed of the net motion along the average swimming direction (i.e., the pitch of the helical trajectory) by dynamically regulating the angular velocity components. Our results suggest that this helical pitch adjustment mechanism is behind the peculiar switching-like behavior. That is, the on response corresponds to the combined effect of helical pitch increase and the attenuation of the periodic component when the direction of motion is mostly aligned with the gradient. In contrast, the off response may be explained as the combined effect of helical pitch decrease when the direction of motion is opposite of the gradient followed by amplification of the periodic component when the direction of motion is misaligned with the gradient. The strength of the off response in our model is determined by the maximum pitch reduction and the peak alignment rate given in Eqs. (22) and (24), respectively. In particular, the off response is most pronounced when $\omega_{\|1}\omega_{\perp 0}^2 \approx \omega_{\|0}\omega^2$, since that leads to zero helical pitch when the direction of motion is opposite of the gradient. Furthermore, the feedback gain in the peak rate alignment depends on the factor $\cos[\phi(\omega)]$, which attains its maximum value when the frequency of the periodic swimming pattern ω is inside the passband of the signaling pathway defined by μ and σ so that the phase lag is minimal. Finally, we remark that the proposed connection between klinotaxis and extremum seeking may guide technological developments in robotic navigation [21,22]; it may inspire engineers to design source seeking algorithms with minimal sensors, suitable for miniaturized robots.

[1] M. Krstic and J. Cochran, Extremum seeking for motion optimization: From bacteria to nonholonomic vehicles, in *2008 Chinese Control and Decision Conference* (IEEE, New York, 2008), pp. 18–27.

[2] B. M. Friedrich and F. Jülicher, Chemotaxis of sperm cells, Proc. Natl. Acad. Sci. **104**, 13256 (2007).

[3] L. Alvarez, B. M. Friedrich, G. Gompper, and U. B. Kaupp, The computational sperm cell, Trends Cell Biol. **24**, 198 (2014).

[4] H. C. Crenshaw, Orientation by helical motion—III. Microorganisms can orient to stimuli by changing the direction of their rotational velocity, Bull. Math. Biol. **55**, 231 (1993).

[5] B. M. Friedrich and F. Jülicher, Steering Chiral Swimmers along Noisy Helical Paths, Phys. Rev. Lett. **103**, 068102 (2009).

[6] J. F. Jikeli, L. Alvarez, B. M. Friedrich, L. G. Wilson, R. Pascal, R. Colin, M. Pichlo, A. Rennhack, C. Brenker, and U. B. Kaupp, Sperm navigation along helical paths in 3D chemoattractant landscapes, Nat. Commun. **6**, 7985 (2015).

[7] U. B. Kaupp, J. Solzin, E. Hildebrand, J. E. Brown, A. Helbig, V. Hagen, M. Beyermann, F. Pampaloni, and I. Weyand, The signal flow and motor response controling chemotaxis of sea urchin sperm, Nat. Cell. Biol. **5**, 109 (2003).

[8] D. A. Priego-Espinosa, A. Darszon, A. Guerrero, A. L. González-Cota, T. Nishigaki, G. Martínez-Mekler, and J. Carneiro, Modular analysis of the control of flagellar Ca2+- spike trains produced by CatSper and CaV channels in sea urchin sperm, PLoS Comput. Biol. **16**, e1007605 (2020).

[9] A. Scheinker, Model independent beam tuning, in *Proceedings of the 2013 International Particle Accelerator Conference, Shanghai, China* (JACoW, CERN, Geneva, 2013).

[10] A. Scheinker and M. Krstić, Extremum seeking with bounded update rates, Sys. Control Lett. **63**, 25 (2014).

[11] J. A. Kromer, S. Märcker, S. Lange, C. Baier, and B. M. Friedrich, Decision making improves sperm chemotaxis in the presence of noise, PLoS Comput. Biol. **14**, e1006109 (2018).

[12] M. Leblanc, Sur l'electrification des chemins de fer au moyen de courants alternatifs de frequence elevee, Revue générale de l'électricité **12**, 275 (1922).

[13] M. Krstic and H.-H. Wang, Stability of extremum seeking feedback for general nonlinear dynamic systems, Automatica-Kidlington **36**, 595 (2000).

[14] K. B. Ariyur and M. Krstic, *Real-Time Optimization by Extremum-Seeking Control* (Wiley, New York, 2003).

[15] A. Abramovici and J. Chapsky, *Feedback Control Systems: A Fast-Track Guide for Scientists and Engineers* (Springer, New York, 2000).

[16] Y. Tan, W. H. Moase, C. Manzie, D. Nešić, and I. M. Mareels, Extremum seeking from 1922 to 2010, in *Proceedings of the 29th Chinese Control Conference* (IEEE, New York, 2010), pp. 14–26.

[17] B. M. Friedrich, I. H. Riedel-Kruse, J. Howard, and F. Jülicher, High-precision tracking of sperm swimming fine structure provides strong test of resistive force theory, J. Exp. Biol. **213**, 1226 (2010).

[18] H. C. Crenshaw, A new look at locomotion in microorganisms: Rotating and translating, Am. Zool. **36**, 608 (1996).

[19] M. Böhmer, Q. Van, I. Weyand, V. Hagen, M. Beyermann, M. Matsumoto, M. Hoshi, E. Hildebrand, and U. B. Kaupp, Ca2+ spikes in the flagellum control chemotactic behavior of sperm, EMBO J. **24**, 2741 (2005).

[20] See Supplemental Material at http://link.aps.org/supplemental/10.1103/PhysRevE.106.L062401 for a full derivation of the quasisteady averaged equations and complete formulas.

[21] J. H. Long, A. C. Lammert, C. A. Pell, M. Kemp, J. A. Strother, H. C. Crenshaw, and M. J. McHenry, A navigational primitive: Biorobotic implementation of cycloptic helical klinotaxis in planar motion, IEEE J. Oceanic Eng. **29**, 795 (2004).

[22] M. Abdelgalil and H. Taha, Recursive averaging with application to bio-inspired 3-D source seeking, IEEE Control Syst. Lett. **6**, 2816 (2022).